

Large enhancement of the in-field critical current density of YBCO coated conductors due to composite pinning landscape

Original

Large enhancement of the in-field critical current density of YBCO coated conductors due to composite pinning landscape / Kihlstrom, Karen Janelle; Civale, Leonardo; Eley, Serena; Miller, Dean; Welp, Ulrich; Kwok, Wai-Kwong; Niraula, Prashanta; Kayani, Asghar; Ghigo, Gianluca; Laviano, Francesco; Fleshler, Steven; Rupich, Martin W; Leroux, Maxime. - In: SUPERCONDUCTOR SCIENCE & TECHNOLOGY. - ISSN 0953-2048. - 34:015011(2021).
[10.1088/1361-6668/ab9f64]

Availability:

This version is available at: 11583/2837589 since: 2020-06-29T14:21:20Z

Publisher:

IOP Publishing Ltd

Published

DOI:10.1088/1361-6668/ab9f64

Terms of use:

This article is made available under terms and conditions as specified in the corresponding bibliographic description in the repository

Publisher copyright

(Article begins on next page)

ACCEPTED MANUSCRIPT

Large enhancement of the in-field critical current density of YBCO coated conductors due to composite pinning landscape

To cite this article before publication: Karen Janelle Kihlstrom *et al* 2020 *Supercond. Sci. Technol.* in press <https://doi.org/10.1088/1361-6668/ab9f64>

Manuscript version: Accepted Manuscript

Accepted Manuscript is “the version of the article accepted for publication including all changes made as a result of the peer review process, and which may also include the addition to the article by IOP Publishing of a header, an article ID, a cover sheet and/or an ‘Accepted Manuscript’ watermark, but excluding any other editing, typesetting or other changes made by IOP Publishing and/or its licensors”

This Accepted Manuscript is © 2020 IOP Publishing Ltd.

During the embargo period (the 12 month period from the publication of the Version of Record of this article), the Accepted Manuscript is fully protected by copyright and cannot be reused or reposted elsewhere.

As the Version of Record of this article is going to be / has been published on a subscription basis, this Accepted Manuscript is available for reuse under a CC BY-NC-ND 3.0 licence after the 12 month embargo period.

After the embargo period, everyone is permitted to use copy and redistribute this article for non-commercial purposes only, provided that they adhere to all the terms of the licence <https://creativecommons.org/licenses/by-nc-nd/3.0>

Although reasonable endeavours have been taken to obtain all necessary permissions from third parties to include their copyrighted content within this article, their full citation and copyright line may not be present in this Accepted Manuscript version. Before using any content from this article, please refer to the Version of Record on IOPscience once published for full citation and copyright details, as permissions will likely be required. All third party content is fully copyright protected, unless specifically stated otherwise in the figure caption in the Version of Record.

View the [article online](#) for updates and enhancements.

1
2
3 Large enhancement of the in-field critical current density of YBCO coated conductors due to
4 composite pinning landscape
5
6
7

8 K. J. Kihlstrom^{1,6}, L. Civale², S. Eley^{2,*}, D. J. Miller¹, U. Welp¹, W. K. Kwok¹, P. Niraula³, A.
9 Kayani³, G. Ghigo⁴, F. Laviano⁴, S. Fleshler⁵, M. Rupich⁵, M. Leroux^{1,2,**}
10
11
12

13 ¹Materials Science Division, Argonne National Laboratory, Argonne, IL 60439, USA
14

15 ²Condensed Matter and Magnet Science, Los Alamos National Laboratory, Los Alamos, NM
16 87545, USA
17

18 ³Department of Physics, Western Michigan University, Kalamazoo, MI 49008, USA
19

20 ⁴Department of Applied Science and Technology, Politecnico di Torino, 10129 Torino, Italy, and
21 Istituto Nazionale di Fisica Nucleare, Sez. Torino, 10125 Torino, Italy
22

23 ⁵American Superconductor Corp., 114 East Main Street, Ayer, MA 01432, USA
24

25 ⁶Physics Department, City University of New York, Queens College, 65-30 Kissena Blvd,
26 Flushing, NY 11367, USA
27

28 * Present address: Department of Physics, Colorado School of Mines, Golden, CO, 80401, USA
29

30 ** Present address: Laboratoire National des Champs Magnétiques Intenses (CNRS, EMFL,
31 INSA, UGA, UPS), Toulouse, 31400, France
32
33

34 35 ABSTRACT

36
37 YBa₂Cu₃O₇-based coated conductors (CCs) achieve the highest critical current densities (J_c) of
38 any known superconductor and are a key technology for applications such as rotatory machines,
39 high-field magnets and power transmission. Incorporation of nano-sized non-superconducting
40 second phases as additional vortex pinning centers has been considered the most amenable route
41 to further enhance J_c at an industrial scale, and has been successfully used in commercial CCs.
42 The resulting pinning landscape is quite complex, with both synergistic and competing
43 interactions among the various types of defects. Particle irradiation, on the other hand, allows for
44 a controlled post-processing incorporation of a well-defined defect morphology. We have
45 previously shown that irradiation with protons and other light ions can further enhance the in-
46 field J_c in commercial state-of-the-art CCs. Here we develop a combined irradiation process that
47 increases J_c above values previously achieved by irradiating with only one species. Our new
48 approach involves sequentially irradiating with 250-MeV Au ions and 4-MeV protons. For
49 example, at $T \sim 27$ K (liquid neon) and $\mu_0 H \sim 4$ T, a region of interest for rotatory machines
50 applications, we obtain $J_c \sim 5$ MA/cm², which is about 40% higher than the values produced by
51 the individual irradiations. Finally, we conclude that this is due to the synergistic pinning effects of
52 the introduced splayed, non-uniform columnar defects and small clusters.
53
54
55
56
57
58
59
60

INTRODUCTION

Coated conductors (CCs), $\text{YBa}_2\text{Cu}_3\text{O}_7$ (YBCO) films deposited on flexible metal tapes, are a leading technology for superconductor applications. CCs can be produced in lengths exceeding 1 km, and are currently being used in prototypes of power transmission lines, motors, generators, fault current limiters and high-field or Tokamak magnets^{1,2,3,4,5,6}. Sustained research has led to tremendous improvement in the performance of CCs, enhancing the critical current density (J_c) by orders of magnitude over pristine YBCO single crystals^{7,8,9,10,11,12,13,14,15,16,17,18,19,20}. In fact, at low temperatures (T) and magnetic fields (H), YBCO films and CCs have the strongest vortex pinning of any known superconductor, with J_c values above 50 MA/cm^2 (e.g. see Ref. 12 & 15), exceeding those in any other superconducting wires (such as NbTi) by at least an order of magnitude²¹. Thus, besides the obvious technological impact, understanding pinning in this extreme case has general scientific interest. Specifically, the rapid decrease of J_c as H increases has thwarted more widespread deployment of CCs, therefore further understanding of vortex matter and improvements in J_c at high fields are critical.

The strong pinning in CCs is a consequence of their mixed pinning landscapes, which are the most effective due to at least two reasons: First, due to changes in the vortex size and density with T and H , different types of disorder will be most effective at pinning vortices in different regions of the H - T phase diagram⁷. Second, some combinations of disorder produce beneficial synergistic effects^{15,22}, such as reducing creep rates. However, the interactions among different types of disorder (such as randomly distributed nanoparticles and point defects, columnar defects, twin boundaries and stacking faults) can also produce detrimental competitive effects^{22,23}.

To further improve the performance of CCs beyond the J_c values achieved by the already quite effective as-grown pinning landscape of “standard” YBCO films⁷, additional disorder must be introduced. There are two common ways to do this: chemical incorporation of non-superconducting second phases^{7,8,9,10,11,12,13,14,15,16,17,18,19,20} and irradiation damage²⁴. The former is now standard in commercial CCs because it has proven industrially-scalable. However, the chemically added defects (e.g. nanoparticles or nanorods) not only interact with, but also alter pre-existing pinning centers, such as twin boundaries and stacking faults, in ways that are difficult to anticipate and control.

Particle irradiation, on the other hand, allows controlled introduction of well-defined types and densities of disorder, thus providing a valuable tool to engineer pinning landscapes and improve our understanding of vortex matter. The nature of the damage produced under different irradiation conditions in YBCO is well known and understood^{25,26,27,28,29,30,31,32}. Numerous studies have been performed on clean single crystals, where the low pre-irradiation J_c can be enhanced by orders of magnitude and the interpretation of the resulting J_c is relatively straightforward^{33,34,35,36,37,38}. However, the use of particle irradiation to improve vortex pinning in coated conductors is relatively unexplored^{39,40,41,42,43,44,45}. Combining different types of

1
2
3 irradiations enables the controlled design of mixed pinning landscapes, but even fewer studies
4 have been published⁴⁶.

6
7 Clearly, since coated conductors display already high J_c , corresponding to a significant fraction
8 of the absolute limit set by the depairing current density, the dramatic increases observed in
9 single crystals are not expected here. Nevertheless, a doubling of J_c at high fields ($\sim 6\text{T}$) and
10 intermediate temperatures ($\sim 27\text{K}$), using post-fabrication proton irradiation, has been obtained
11 in commercial CCs³⁹. Even more remarkable was the subsequent demonstration that essentially
12 the same beneficial effects could be obtained by oxygen irradiation using a dose 3 orders of
13 magnitude smaller⁴⁰. This allowed the irradiation to be done at a rapid rate of just one second per
14 cm^2 , compatible with the tape speed on a CC production line, thus enabling the use of this tool at
15 industrial scale. Indeed, broad J_c improvements using reel-to-reel 16-MeV Au^{5+} irradiation of 46-
16 mm wide production tapes were subsequently achieved⁴¹.

19
20 Here, we further build on those previous studies^{39,40,41,42} by exploring the pinning effects of
21 compound defects, introduced in production line CCs by irradiation with 250-MeV gold ions and
22 4-MeV protons. We achieve J_c values that surpass those previously reached with proton
23 irradiation and extend over a much wider field range ($J_c \sim 13 \text{ MA/cm}^2$ and 6 MA/cm^2 at 27K in
24 applied fields of $1\text{T}||c$ and $6\text{T}||c$, respectively). We use the T and H dependencies of J_c and the
25 vortex creep rates (S) to investigate the contribution of the two types of disorder and the synergy
26 between them.

28 29 EXPERIMENTAL DETAILS

30
31 The samples studied here are Dy-doped YBCO films manufactured by American Superconductor
32 Corp (AMSC), with nominal thickness $\delta=1.2 \mu\text{m}$ (based on a YBCO coating of 7200 mg/m^2 and
33 excluding porosity and added Dy_2O_3), deposited by MOD (metal organic deposition) onto
34 RABiTS™ substrates (Rolling Assisted Bi-axially Textured Substrates)^{16,39,40,41,42,47}. All samples
35 are capped with a $0.8 \mu\text{m}$ thick Ag-layer protecting the superconducting film. The samples were
36 irradiated with 250-MeV gold ions (Au^{+17}) along the c -axis at room temperature to a dose-
37 equivalent matching field $B_\phi=3\text{T}$, using the Tandem-XTU facility of the LNL laboratories of the
38 Italian National Institute for Nuclear Physics (INFN). The ion beam was normal of the YBCO
39 CCs (parallel to the c -axis), and the ion flux was kept below $1.8 \times 10^8 \text{ cm}^{-2} \text{ s}^{-1}$ to avoid sample
40 damage due to heating. After characterization, these samples were irradiated with 4-MeV protons
41 along the c -axis at the 6-MV tandem van de Graaff accelerator at Western Michigan
42 University^{39,40}. A gold foil was used to homogenize the beam over an area of $\sim 1 \text{ cm}$ diameter,
43 and typical p-beam currents of $0.5 \mu\text{A}$ were used, in addition to a cooling stage to prevent sample
44 heating. All irradiations occurred through the protective Ag-layer.

48
49 Magnetization (M) studies were performed in two commercial Quantum Design SQUID
50 magnetometers using $3 \times 5 \text{ mm}^2$ rectangular samples, patterned by photolithography and Ar-ion
51 milling. One of the magnetometers was used to measure $M(H)$ loops at various T for $\mathbf{H}||c$ -axis,
52 i.e., normal to the film surface, and $J_c(H,T)$ was determined from the width of the hysteresis, ΔM ,
53 using the Bean critical state model⁴⁸. The second magnetometer was used to investigate the flux
54 creep as a function of T and H , for $\mathbf{H}||c$ -axis. To prepare an initial fully penetrated critical state
55
56
57
58
59
60

for the creep studies, first a large enough negative field was applied, then the field was swapped to the measuring field $H > 0$ and a few data points (typically 8) were measured in this *field increasing* or *lower* branch⁴². Subsequently the field was increased to a high enough positive value and finally decreased again to the measuring H , where the time decay of \mathbf{M} on this *field decreasing* or *upper* branch was recorded over a period of ~ 1 hour. The initial points on both branches were averaged to obtain \mathbf{M}_{avg} , which was subtracted from \mathbf{M} to obtain the irreversible contribution \mathbf{M}_{irr} associated with the critical state, and the creep rates were calculated as $S_{1,t} = -d(\ln M_{\text{irr},t})/d(\ln t)$. Transport measurements at 27K were performed using conventional four-terminal geometry on 0.065 mm x 4.0 mm bridges patterned by photolithography and Ar ion milling.

Characterization of the defect structure was carried out using high-resolution and diffraction contrast transmission electron microscopy (TEM)^{39,40}. TEM samples were prepared by focused ion beam (FIB) lift-out methods followed by low-energy Ar ion milling. This approach minimizes artifacts due to specimen preparation. Several TEM samples were prepared from different regions of each sample to ensure that results were representative of each condition. The pinning landscape of pristine MOD-CCs, such as those used in this study, is already very complex. As shown in the TEM image in Fig. 1a, it contains randomly distributed Dy_2O_3 nanoparticles (NPs) that are $\sim 30\text{nm}$ in diameter, which are purposely introduced during fabrication, in addition to a small density of larger $\text{Y}_2\text{Cu}_2\text{O}_5$ NPs, twin boundaries and stacking faults, all of which appear spontaneously during synthesis^{16,42,47}. There are also point defects, not visible in the TEM images.

RESULTS AND DISCUSSION

I. Microstructure

Proton irradiation has been extensively used to enhance the vortex pinning in superconductors³³. Earlier TEM work on YBCO showed that p^+ irradiation produces a hierarchy of randomly distributed defects with sizes ranging from atomic scale (Frenkel pairs), mostly on the O and Cu sites, to clusters that are 2-5 nm in diameter^{29,39,42}. A typical TEM image for a p^+ -irradiated sample³⁹ similar to the pieces used in this study is shown in Fig. 1b. Ultimately, the reason for the effectiveness of p^+ or other light-ion irradiations (such as O) is that pinning in the pristine AMSC CC is dominated by the Dy_2O_3 NPs, which are particularly effective at low fields where the intervortex distance is of the order of, or larger than, the average distance among NPs. At higher H there are not enough NPs and their effectiveness decreases. At near-optimum p^+ doses the densities of the smaller irradiation-induced defects are orders of magnitude higher than that of the NPs, allowing the irradiation induced defects to remain effective pinning centers at high H .

II. Critical current

Fig. 2 shows the dose dependence of J_c in our proton-irradiated CC sample. Due to the competition between increasing pinning force and decreasing superconducting volume fraction, a non-monotonic dependence of J_c on irradiation dose, i.e. pinning sites concentration, is theoretically expected⁴⁹. This behavior is observed in Fig. 2. We found that, although J_c reaches

its maximum at a dose that is temperature and field dependent, a dose of $\sim 18 \times 10^{16}$ p/cm² is a good compromise over a broad T and H range that is technologically relevant. Note that this relatively high dose of irradiation only induces a modest reduction of T_c . As shown in Fig. 3a, the suppression rate of T_c is only 0.2 K per 10^{16} p/cm², which is much less than in single crystals. Also, no broadening appears in the magnetization curves around T_c (Fig. 3b) evidencing the homogeneity of the irradiations. A possible reason for this small suppression rate of T_c in coated conductors is that the numerous big defects and nanoparticles, which are already present in the pristine sample, act as sinks for the mobile point defects induced during irradiation. Isolated point defects are indeed the type of defects with the strongest impact on T_c (pair-breaking from electronic scattering in a d-wave), whereas the large columnar defects and clusters are much bigger and thus are weaker scattering centers i.e less “pair-breaking”⁶⁶.

Fig. 4 shows J_c vs. H at four temperatures, as obtained from magnetization measurements for a pristine piece of CC (black squares) that was subsequently irradiated with Au (red circles) then protons (blue diamonds), as well as a piece from the same batch that was irradiated to 18×10^{16} p/cm² (green triangles). This last piece is the one that was studied after repeated irradiation in Fig.2. We first note that at $T=5$ K (Fig. 4a) and $H \sim 0$, the J_c of this CC is higher than the J_c reported for YBCO single crystals irradiated at any conditions. We also observe the typical fast decay in $J_c(H,T)$ as H or T are increased.

In Figs. 5a-d we plot the field dependence of the J_c enhancement factors, $J_c(H,T)/J_c^{pristine}(H,T)$ for the same temperatures as in Fig. 4 so as to facilitate the comparison of the effectiveness of proton, gold and gold+proton irradiations. Firstly, let us consider the optimum 4-MeV p⁺ irradiation: from Figs. 4a-c and 5a-c, we see that for $T \leq 50$ K the effect goes from detrimental to beneficial (i.e., J_c increases as compared to the pristine sample) above a crossover field H_{cr} , with $\mu_0 H_{cr} \sim 0.6$ T at 5K (Figs. 4a and 5a), increasing to ~ 1 T at 50K (Figs. 4c and 5c). For $T = 77$ K, the effect of the (optimum) p⁺ irradiation is detrimental at all fields (Figs. 4d and 5d). This suppression of J_c at low H following p⁺ irradiation is likely caused by competing (as opposed to synergistic) pinning effects. Creep studies show that such competition arises at least in part from faster creep due to lower activation energies following irradiations⁴².

Now, let us consider the case of Au irradiation. Columnar defects (CDs) produced by swift heavy-ion irradiation are the most effective pinning centers for H||CDs and below the matching field ($B\Phi$), because the whole length of the cores of all the vortices can be trapped³⁶. They also retain their effectiveness up to higher T than point defects, due to their larger pinning energy. For both reasons, they are natural candidates to complement the effect of the p⁺ irradiations.

As a first step in our combined irradiation landscape engineering, we irradiated our sample with 250 MeV Au ions. We selected this relatively low energy heavy-ions to create CDs that are *splayed* and *inhomogeneous* along their length, because these features are known to produce the beneficial effect of slowing down the vortex dynamics due to low-energy kink excitations^{15,50,51}, as will be described below. The presence of CDs with these characteristics is clearly observed in Figs. 1c-d, which were obtained on the piece of CC used in this study after all irradiations and measurements were completed. The diameter of the CDs is ~ 7 -8 nm, somewhat larger than the

diameter of the vortex cores, $2\sqrt{2}\xi_{ab}(T)$, which is $\sim 5\text{nm}$ for YBCO at $T \ll T_c$, making them effective pins (here ξ_{ab} is the in-plane coherence length). We chose a dose-equivalent matching field $B_\Phi = 3\text{T}$ which is somewhat lower than the optimum B_Φ for J_c enhancement reported in the literature for YBCO⁵², and is also in the range of target magnetic fields for rotating machinery applications¹.

The red symbols in Figs. 4 and 5 show J_c and $J_c/J_c^{\text{pristine}}$ respectively, after the 250 MeV Au ions irradiation. The dissimilar effects of the p^+ and Au irradiations are apparent. First, for $T \leq 27\text{K}$ the Au irradiation produces no detrimental effect at low H ; in fact there is even a small increase in $J_c(H=0, T=5\text{K})$ (Figs. 4a-b and 5a-b). For $T=50\text{K}$ a slight deterioration occurs at low field, but it is less pronounced than for p^+ and H_{cr} is much smaller (Figs. 4c and 5c). For $T \leq 50\text{K}$ the enhancement factor for the Au irradiation first increases with H , similarly to the p^+ irradiation, but then maximizes at an intermediate field $\sim 1.5\text{T} - 2\text{T}$ and, in contrast to the p^+ case, decreases for higher fields as most CDs become occupied and vortices in between the CDs start to proliferate. At $T = 5\text{K}$, the 250-MeV Au processing becomes less effective than the 4-MeV p^+ processing at $\sim 4\text{T}$, i.e. just above B_Φ . However, as T increases the larger pinning energy of the CDs (due to their longer length) comes into play such that at 27K the CDs remain better up to $\sim 5\text{T}$, and at 50K they remain superior all the way up to our maximum field.

The $T = 77\text{K}$ results (Figs. 4d and 5d) deserve particular consideration. First, the low H deterioration is as bad for Au as for p^+ irradiation, with $J_c(H \sim 0, T = 77\text{K})/J_c^{\text{pristine}}(H \sim 0, T = 77\text{K}) \sim 0.5$, and T_c suppression is also similar in both cases: 88.4 K and 87.3K respectively, see Fig. 3. However, at high H the Au irradiation does improve J_c , in sharp contrast to the p^+ case. It must be recognized that the dramatic enhancement factors (>10) at high H are a consequence of the very small J_c of the pristine sample. Nevertheless, a critical current density $J_c(H=4\text{T}, T=77\text{K}) \sim 0.1 \text{ MA/cm}^2$ is encouraging and would enable applications of CC refrigerated by liquid N_2 .

The fact that the Au irradiation has almost no effect at $H \sim 0$ and low T is not trivial and clearly evidences that pinning is not additive. At low fields, a material may have enough strong pinning centers to pin all the vortices very effectively. In a simple scenario, adding weaker defects will not create better pinning configurations; vortices will just “ignore” them and J_c will be unaltered. The rich landscape of the pristine CC contains a small density of pinning centers (or combinations of them) that are very strong. As H increases those few defects become saturated and the much larger density of CDs progressively increase their fractional contribution to J_c , as we observed. We know, however, that this cannot be the complete picture, as, in contrast to Au irradiation, p^+ irradiation decreases J_c at $H \sim 0$ as already discussed.

After examining the effect of proton and Au irradiation independently we combined both: the piece irradiated with Au was also irradiated with 4-MeV p^+ . We selected a dose of $4 \times 10^{16} \text{ p/cm}^2$, well below the optimum for p^+ irradiation alone to avoid excessive damage, but large enough to produce significant J_c enhancement in a pristine CC, as shown by the right dashed line in Fig. 2. The small defect clusters created by this second irradiation are visible in Fig. 1d. Note that it is well-known that p^+ irradiation also creates point defects, but these are not visible in these TEM

1
2
3
4 images. The resulting $J_c(H,T)$ and $J_c(H,T)/J_c^{pristine}(H,T)$ curves are shown as blue diamonds in
5
6 Figs. 4 and 5 respectively. It is apparent that the mixed landscape created by this *combined*
7
8 *irradiation* produces better performance than either the 250-MeV Au or the 4-MeV p^+ alone. The
9
10 yellow colored areas in Fig. 5 highlight the additional synergistic J_c enhancement produced by
11
12 the combined irradiations, as compared to either of the individual ones. Below $\sim 1T$ and for all T ,
13
14 the J_c resulting from the combined irradiation process is marginally smaller than the Au result,
15
16 but for $\mu_0H > 1T$ and $T \leq 50K$ it produces clearly stronger pinning. As seen in Fig. 5b, for $T =$
17
18 $27K$ and fields in the 4-6T range, a regime particularly relevant for superconducting rotatory
19
20 machines, the combined irradiation exceeds the effect of the individual ones by roughly a factor
21
22 of two. This unforeseen synergetic effect is the central result of this study. In Fig.2, one can also
23
24 see that at $27K / 4T$ a proton irradiation dose of $4 \cdot 10^{16} p/cm^2$ should yield $J_c \sim 3.5 MA/cm^2$ and
25
26 from Fig.4b one can see that the $B_\phi=3T$ Au irradiation also yields $J_c \sim 3.8 MA/cm^2$ at $27K / 4T$.
27
28 Hence, the value $J_c \sim 5.1 MA/cm^2$ of the combined irradiations ($B_\phi=3T$ Au + $4 \cdot 10^{16} p/cm^2$) is
29
30 about 40% higher than either individual irradiations. We believe this synergy stems from the
31
32 concept of a mixed pinning landscape^{22,39}, in which the randomly distributed localized defects
33
34 from proton irradiation catch stray vortices and suppress vortices jumping between CDs (for
35
36 instance by hampering double kinks expansion, cf. part III). For $T = 77K$, the combined
37
38 irradiation just replicates the Au irradiation result, which confirms the ineffectiveness of p^+
39
40 irradiation induced defects at 77 K, as already observed in Fig. 2.

41
42 In summary, at intermediate magnetic fields and all temperatures in Fig.4, the blue curve of
43
44 combined Au and proton irradiation is above all others thanks to the synergy between defects.
45
46 Then at high magnetic field and low temperature the best pinning centers are the numerous
47
48 clusters and Frenkel pairs generated by proton irradiation which can accommodate a large
49
50 number of vortices³⁹, whereas the columnar defects from gold irradiation are saturated with
51
52 vortices above the matching field of 3T. Hence in Fig.4 the green curve ($18 \times 10^{16} p^+/cm^2$) shows
53
54 higher J_c than the red curve (Au, $B_\phi=3T$) at high magnetic field and low (a) or intermediate (b)
55
56 temperature. At high temperature (77 K, Fig.4(d)) however, the defects from proton irradiation
57
58 are too small and weak to pin vortices efficiently whereas the long columnar defects retain their
59
60 strong pinning properties.

41
42 Finally, to confirm that the CDs produced by Au irradiation indeed act as correlated pinning
43
44 centers in our samples, we performed angular-dependent transport studies of J_c on a bridge
45
46 patterned from the same CC batch. Fig. 6 shows J_c vs. the angle between \mathbf{H} and the c-axis (Θ), at
47
48 $T = 27K$ and $\mu_0H = 6T$, for that bridge before and after irradiation with 250-MeV Au to a dose
49
50 equivalent $B_\phi=3T$. In the pristine state, $J_c(\Theta)$ shows the typical anisotropy of AMSC CCs, with a
51
52 large maximum centered at $\mathbf{H} \parallel ab$ associated with correlated pinning by stacking faults, and a
53
54 small c-axis peak due to twin boundaries. After irradiation, a much larger c-axis peak
55
56 demonstrates the correlated pinning of the artificial CDs.

53 III. Vortex creep

54
55
56
57
58
59
60

Additional information about the pinning landscape can be obtained from the vortex dynamics, in particular from the normalized flux creep rates^{53,54,55} $S(T,H)$. Such information is complementary because of the quite different dependences of J_c and S on disorder. The former is very sensitive to the details of the pinning landscape, and consequently J_c values differing by orders of magnitude, as well as countless variations of the $J_c(T,H,\Theta)$ functional dependences, have been reported for YBCO. In contrast, creep rates in YBCO exhibit much less variability, with absolute values that are similar in all cases and functional dependences that typically fall into one of a few categories.

The reason for this is that $S(T,H)$ is mainly defined by the type of the dominant depinning excitations, rather than by the quantitative values of the pinning parameters⁵⁴. First, the dynamics can be either glassy or plastic^{56,57,58}. In the first case the size of the excitation (either a vortex segment or a vortex bundle) diverges in the limit of $J \rightarrow 0$, and consequently the flux creep activation energy diverges as $U(J) \propto U_p \times (J_c/J)^\mu$, where $U_p(T,H)$ is the pinning energy and $\mu > 0$ is the glassy exponent. In the second case, in contrast, the size and the activation energy of the excitation remain finite for $J \rightarrow 0$ and the low J behavior $U(J) \propto U_p \times (J_c/J)^p$ is characterized by a plastic exponent $p < 0$. Within each category, different excitations produce different exponents. For instance, in collective pinning due to random point disorder: $\mu = 1/7, 3/2$ or $7/9$ depending on the regime⁵⁷. Depinning due to the excitation of half-loops associated with CDs have⁵⁹ $\mu = 1$. The traditional Anderson-Kim (AK) regime has⁵³ $p = -1$. The numerical values of U_p and J_c have limited influence on the values of S . Mathematically, this stems from the fact that S is defined by logarithmic derivatives. These values determine the crossovers among creep regimes in the T - H phase diagram.

Several examples of the most common flux creep regimes for YBCO are illustrated in Fig. 7, where $S(T)$ at 1T for $H \parallel c$ is plotted for seven samples with dissimilar pinning landscapes. We first note that, for a given T , all the samples (with the exception of sample #C, discussed below) have S values within a factor of two of each other, in spite of the fact that their J_c 's span a range of almost two orders of magnitude, particularly at high T .

At low T up to $\sim 10K$, all samples have similar creep rates, with $S(T)$ increasing monotonically with T . This is the AK regime in which, as we have shown recently⁶⁰, creep for all YBCO samples is close to the universal lower limit given by $S_{AK}(T) \sim Gi^{1/2}(T/T_c)$, where Gi is the Ginzburg number. In addition, there is a nonzero $S(T \rightarrow 0)$ extrapolation that is frequently attributed to a T -independent quantum creep component S_Q . At high T (above $\sim 60K$), $S(T)$ for all samples increases fast with increasing T , signaling the crossover from glassy to plastic creep⁵⁸ and the approach to the irreversibility line.

At intermediate T (between $\sim 10K$ and $\sim 60K$), there are basically three types of $S(T)$ curves. Many samples exhibit a large T -independent "plateau" arising from the glassy 3D collective pinning regime of vortex bundles⁶¹, $S \sim [\mu \ln(t/t_0)]^{-1}$, where t_0 is a microscopic attempt time. Examples for this behavior are seen in samples A and E in Fig. 7, both of which have pinning dominated by random distributions of point defects or small clusters, although the density of such defects is far greater in E than in A. The second category consists of samples with CDs,

which develop a maximum in $S(T)$ at intermediate T arising from the expansion of double kinks^{50,51,54,59,62}. In the case of perfectly parallel CDs, initial double-kink expansion should not be glassy⁶³ (because the kinks have finite sizes) and should turn glassy with a low $\mu \sim 1/3$ (at low H) as J decreases^{50,51,59,62,63}. The result is a very large $S(T)$ peak as in the case of the single crystal C, where CDs with negligible splay were produced by very energetic heavy-ions (1 GeV Au)⁵¹. A number of strategies can be used to reduce the height of the technologically undesirable $S(T)$ peak by moderating the double-kinks expansion. The first option is to introduce splay among the CDs^{50,51} to geometrically constrain the kinks propagation. An example of this situation is realized in sample B, a single crystal with splayed CDs produced by less energetic ions (0.6 GeV Sn). The double-kinks peak is still clearly visible, but it is smaller than in A. The second option is the incorporation of localized defects in between the CDs¹⁵ to pin the kinks. Sample F, a film grown by Pulsed Laser Deposition containing splayed self-assembled BaZrO₃ nanorods as well as randomly distributed nanoparticles, is an example of combining both strategies, and consistently the peak is even smaller than in B. The third category of $S(T)$ curves are MOD films with pinning dominated by randomly dispersed nanoparticles^{42,58,64}, which exhibit a minimum in $S(T)$ at low H and intermediate T , as our pristine film D (the minimum is more pronounced at lower H , see fig. 6 in ref. 42). In several previous studies, we have observed that irradiation of the MOD films with light particles that introduce point defects and small clusters increases S at low H and intermediate T , eliminating the minimum and recovering the plateau (sample E)^{39,40,41,42}.

Finally, curve G in Fig. 7 corresponds to our combined-irradiation CC. These data show the characteristic $S(T)$ peak due to CDs, but the height is smaller than for sample B. Similarly to the case of sample F, this strongly reduced double-kink expansion, which is technologically desirable, is due to the combination of the two factors discussed above, namely, CDs that are splayed and inhomogeneous along their length as well as the presence of p-irradiation induced additional defects to pin the kinks.

Fig. 8 shows $S(T)$ curves for the combined irradiation sample at several fields, as well as the $\mu_0 H = 1T$ curve for the pristine film D shown in Fig. 7 (dashed red curve). The double-kink peak is expected to be highest at the lowest fields, when vortex-vortex interactions can be neglected and each vortex pinned in a CD has plenty of nearby unoccupied CDs where kinks can propagate. This is the condition where the initial non-glassy and later glassy with $\mu=1/3$ dynamics is expected^{50,51,59,62,65}. It has been shown⁵⁰ that splay should increase the glassy exponent to $\mu \sim 0.6$, thus reducing the height of the peak from $S \sim [\mu \ln(t/t_0)]^{-1} \sim 0.11$ to ~ 0.05 . Unfortunately, there are no theoretical estimates for μ in the presence of localized disorder in between the CDs, nor of how both effects would combine. In any case, we can take the maximum $S \sim 0.036$ for $\mu_0 H = 0.3T$ to estimate $\mu \sim 0.9$. Vortex-vortex interactions will stiffen the lattice, reducing S . Interactions will increase with increasing T , due to the increase of the transverse vortex localization length and the proliferation of kinks, producing the observed decrease in $S(T)$ with increasing T after it peaks, see Figs. 7 and 8. Increases in H will also increase the interactions, producing two effects: the $S(T)$ peak will shift to lower T and decrease in height. Both expectations are clearly observed in Fig. 8; in particular, as shown in the inset, the peak vanishes above $B_\Phi = 4T$ when all CDs are

1
2
3 occupied and individual vortex double kink propagation stops (and are replaced by vortex bundle
4 excitations).
5

6
7 Comparison of the $\mu_0 H = 1\text{T}$ curves for the pristine and irradiated CCs in Fig. 7 (curves D and
8 G) and Fig. 8 shows that they are similar for $T \leq 15\text{K}$. This is fully consistent with the
9 observation that the double irradiation does not significantly affect J_c at low T and H , as
10 discussed before. It is also clear that the minimum in $S(T)$ at $\sim 45\text{K}$ associated with NPs, well
11 developed in the pristine sample, disappears after irradiation. This is consistent with our previous
12 finding that, for the $S(T)$ minimum to occur, NPs not only have to be present, they must be the
13 *dominant* pinning source⁴². Finally, it is worth noticing that in Fig. 8, outside the T - H regions
14 where the dynamics is dominated by double kinks or NPs, all the $S(T,H)$ data converges into a
15 narrow plateau at $S \sim 0.025$ (light yellow band) corresponding to the “standard” collective creep
16 of bundles ($\mu \sim 1.3$), and suggesting that the dynamics is dominated by point and small-clusters
17 defects.
18
19

20 21 CONCLUSION

22
23 YBCO-based CCs constitute the extreme case of the present capability to create an effective
24 vortex pinning landscape. Successful nanoengineering of the disorder to produce any further J_c
25 enhancement is a hard materials science challenge that requires a deep understanding of the
26 many body system formed by the interacting vortices and the complex defects structure. We
27 have shown that the performance of commercial CCs with artificial pinning centers (chemically
28 incorporated second-phase nanoparticles) can be further improved by combining irradiations
29 with swift Au ions and few MeV protons, which create splayed, non-uniform columnar defects
30 and a combination of point and small-cluster defects, respectively. The resulting J_c s show
31 striking synergies and are higher than those achieved by any of the individual irradiations, in
32 particular in the region of magnetic fields of a few Tesla and intermediate temperatures that is
33 relevant for applications. The effectiveness of this pinning landscape is a consequence of the
34 synergistic pinning effects among the defects of different morphology and hints that even further
35 performance improvements may be possible.
36
37
38

39 40 ACKNOWLEDGEMENTS

41
42 Particle irradiation, measurements of vortex creep and magnetization hysteresis and their
43 analysis were supported as part of the Center for Emergent Superconductivity, an Energy
44 Frontier Research Center funded by the U.S. Department of Energy, Office of Science, and
45 Office of Basic Energy Sciences. Angular dependent magnetoresistance measurements were
46 supported by the U. S. Department of Energy, Office of Science, Basic Energy Sciences,
47 Materials Sciences and Engineering Division. Electron microscopy was performed in the
48 Electron Microscopy Center at the Center for Nanoscale Materials, a U.S. Department of Energy
49 Office of Science User Facility under Contract No. DE-AC02-06CH11357. S. E. acknowledges
50 support from the National Science Foundation under Grant No. 1905909 (manuscript
51 preparation).
52
53
54
55
56
57
58
59
60

1
2
3
4
5
6
7
8
9
10
11
12
13
14
15
16
17
18
19
20
21
22
23
24
25
26
27
28
29
30
31
32
33
34
35
36
37
38
39
40
41
42
43
44
45
46
47
48
49
50
51
52
53
54
55
56
57
58
59
60

Accepted Manuscript

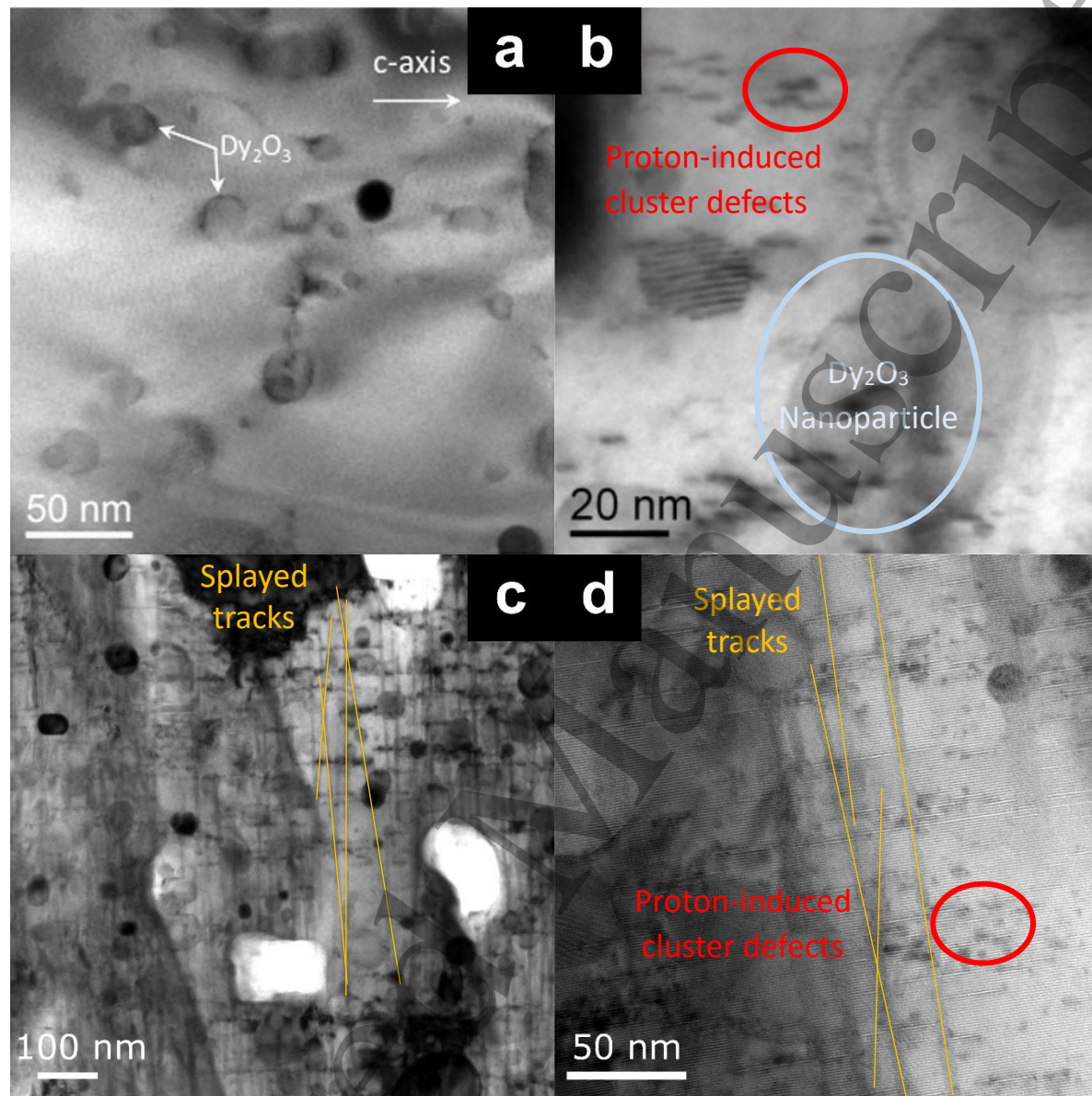
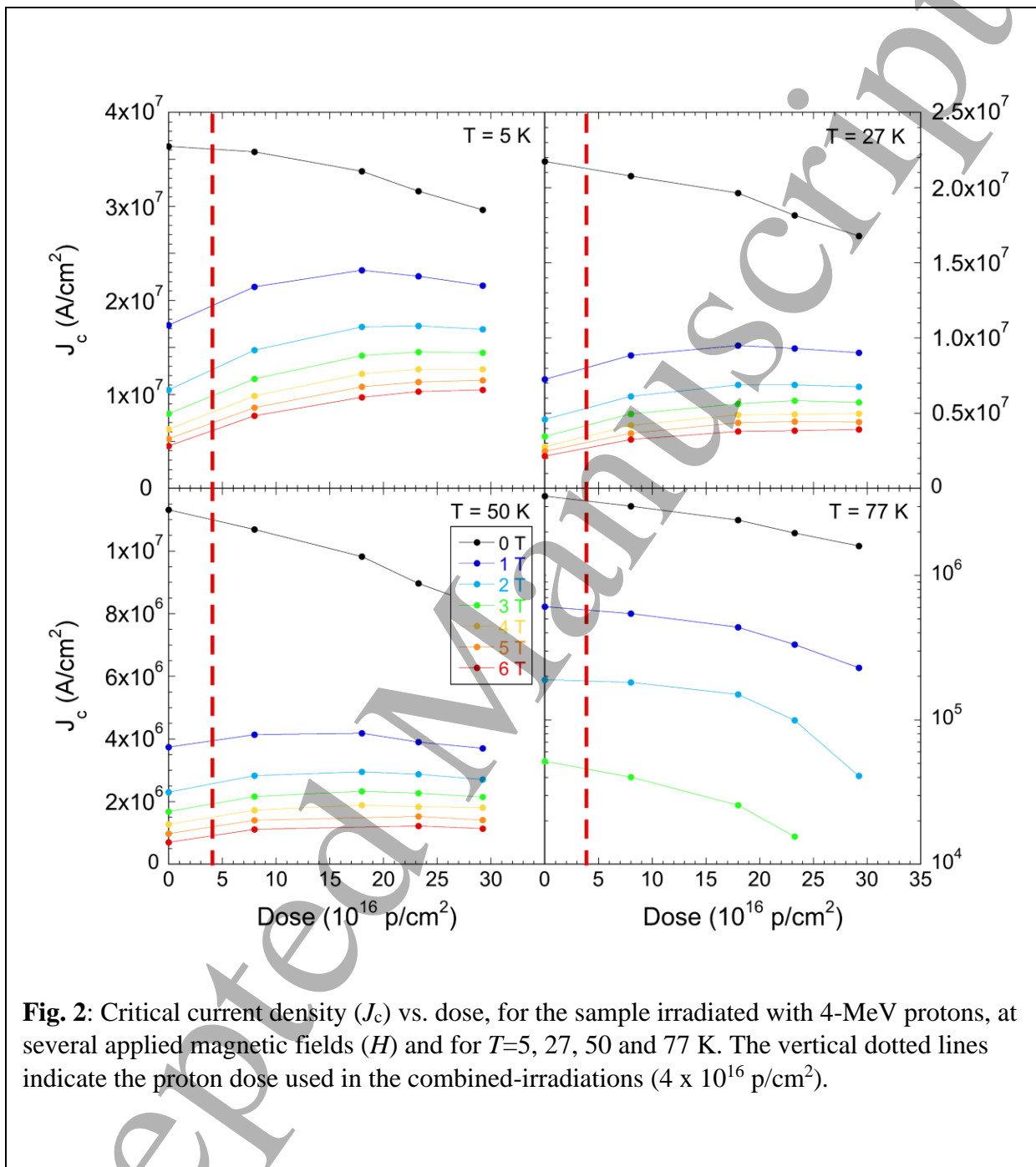


Fig. 1: Bright field TEM images representative of the samples studied in this paper: (a) a pristine as-grown MOD-CC with Dy_2O_3 nanoparticles; (b) a proton irradiated MOD-CC, with $\sim 5\text{nm}$ sized irradiation-induced clusters. (c-d) a CC piece with compound defects: splayed, non-uniform tracks $\sim 7\text{nm}$ in diameter created by Au irradiation and small defect clusters created by proton irradiation. Image (a) reproduced from Ref. 42. Image (b) reproduced from Ref. 39 Appl. Phys. Lett. **103**, 122601 (2013) (<https://doi.org/10.1063/1.4821440>), with the permission of AIP Publishing.



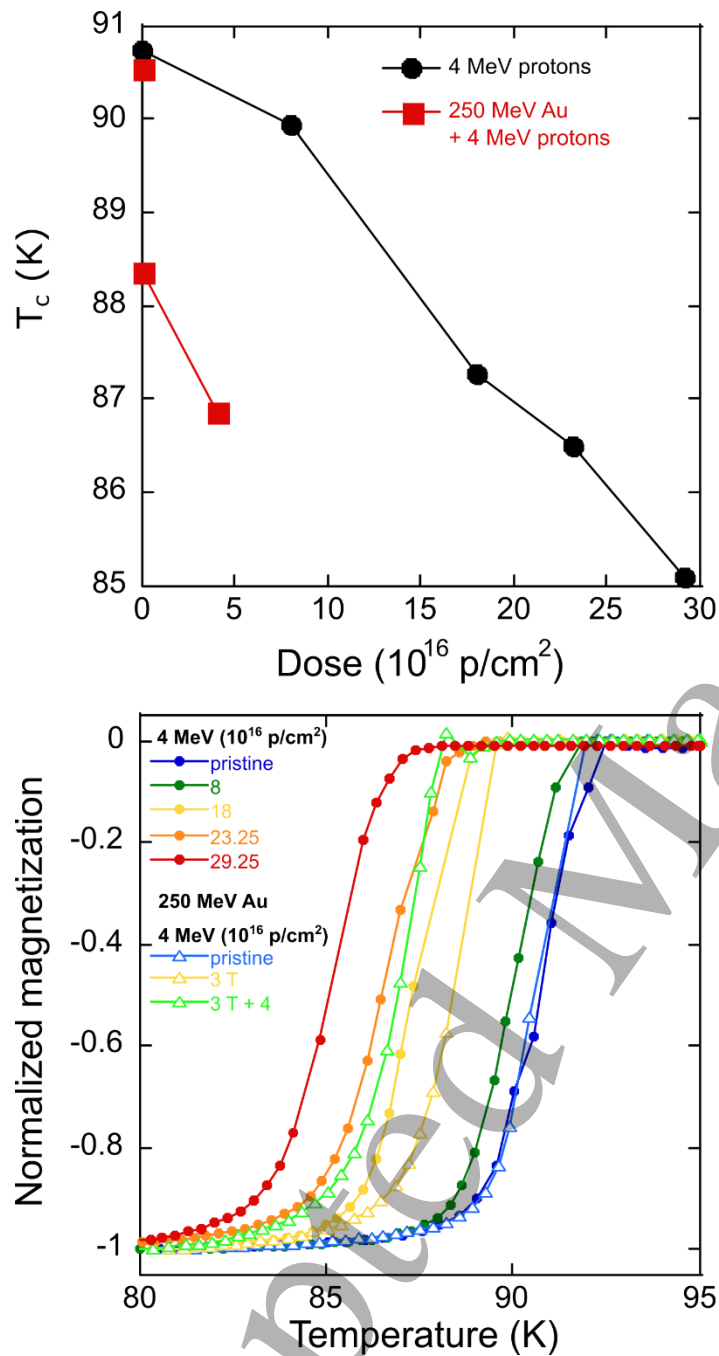


Figure 3 (a) Critical temperature as a function of proton irradiation dose for both the proton-irradiated sample and the combined Au+proton-irradiated sample. (b) Magnetization measurements from which T_c was determined. The labels indicate the p+ (circles), Au (triangles), and combined doses (green triangle).

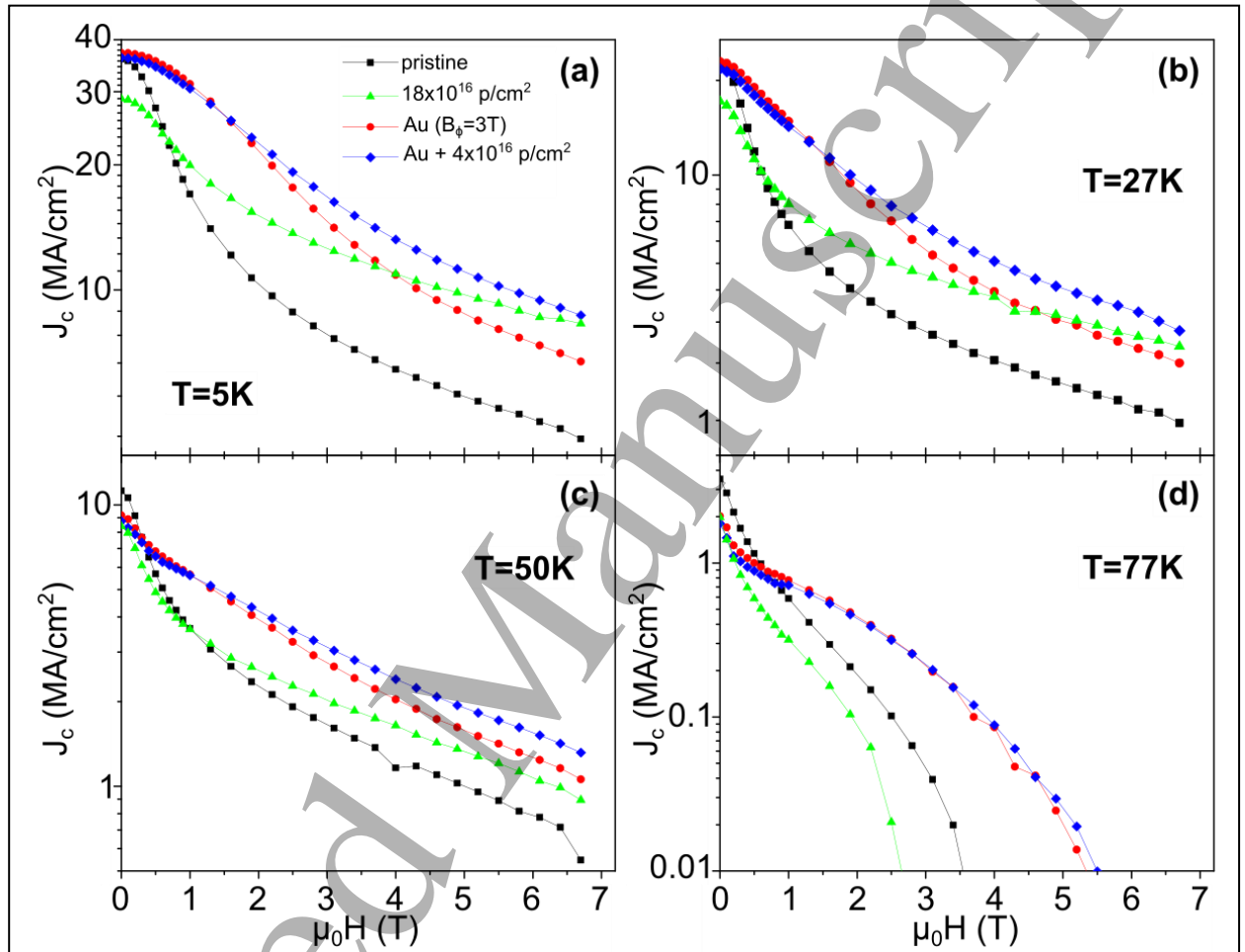
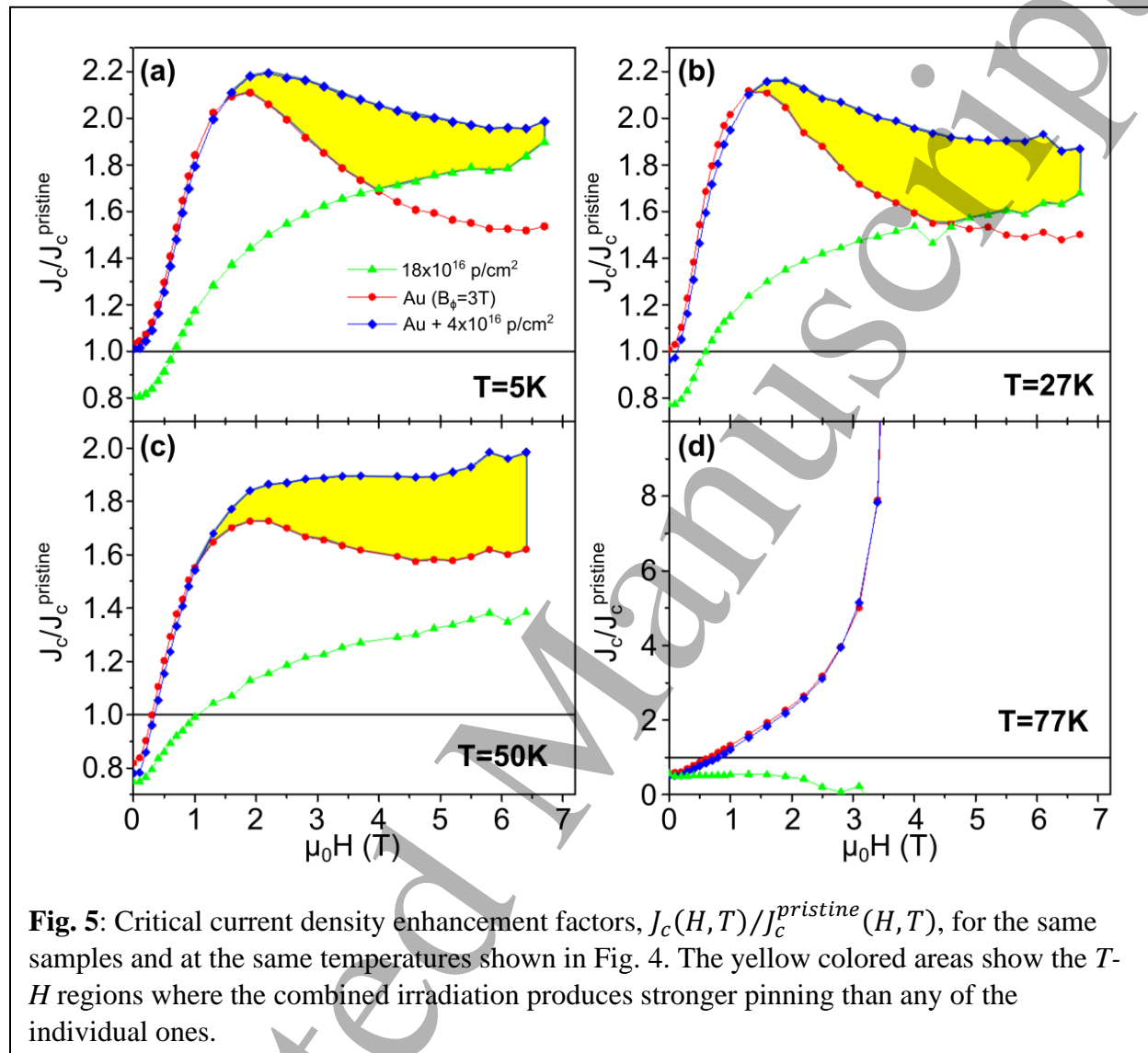


Fig. 4: Critical current density (J_c) measured by magnetization vs. applied magnetic field (H) at four temperatures, in samples from the same batch, for: (black squares) a pristine CC; (green triangles) a CC irradiated to the optimum proton dose (see text); (red circles) a CC piece irradiated with Au; and (blue diamonds) the same CC piece after both Au and proton irradiation.



Accepted

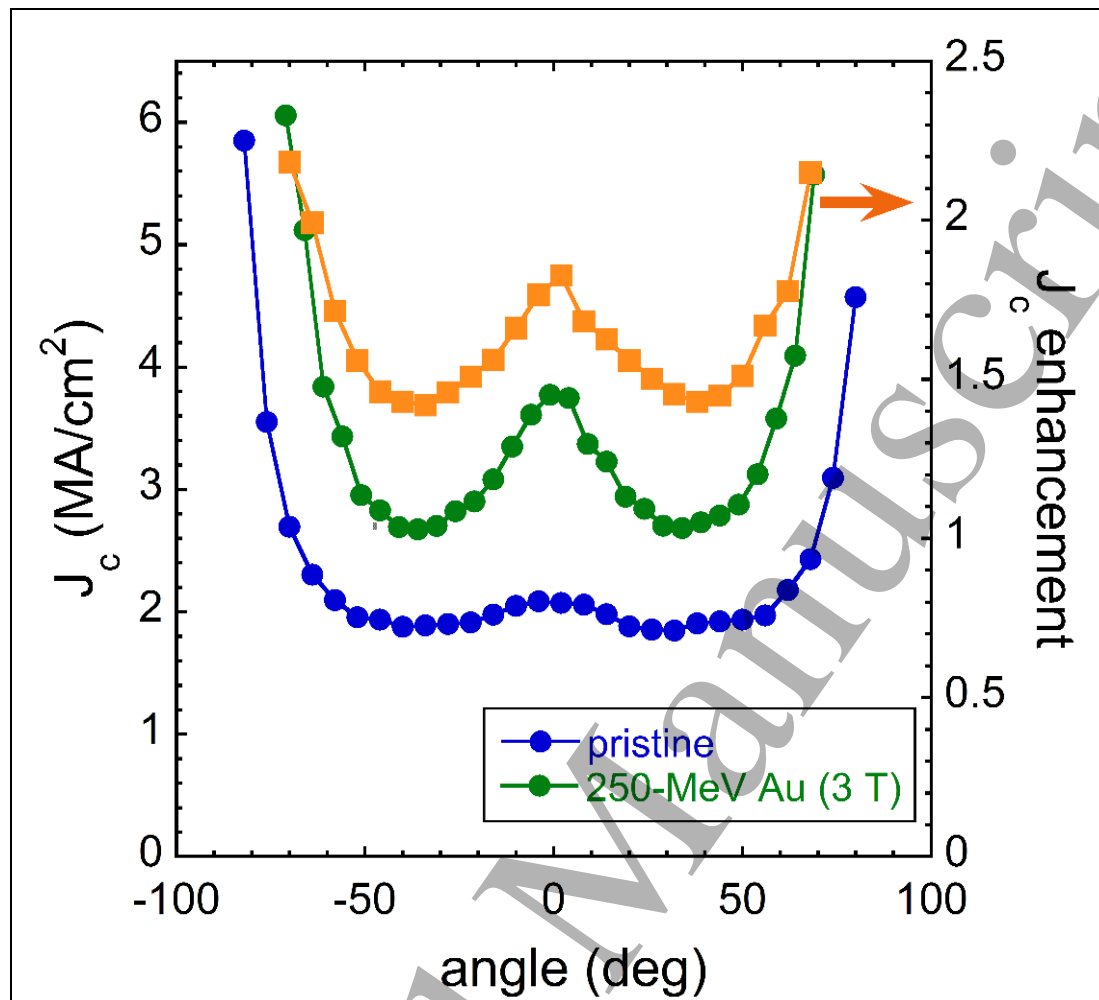
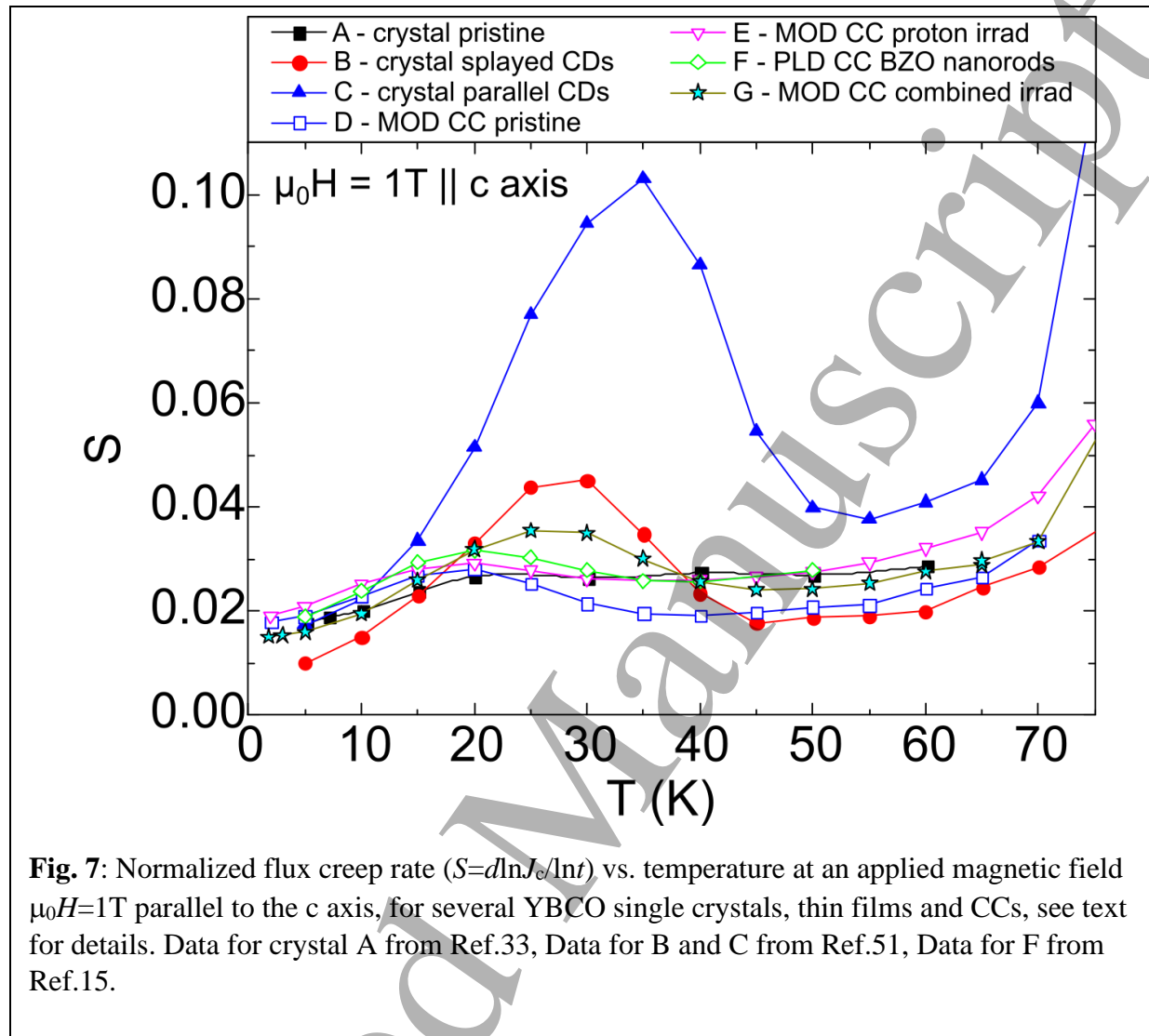


Fig 6: Critical current density (J_c) measured by transport vs. applied magnetic field orientation at $T=27\text{K}$ and $\mu_0 H=6\text{T}$ for a CC from the same batch as the samples shown in Figs. 2 and 4, before (blue curve) and after (green curve) 250 MeV Au irradiation to $B_\Phi = 3\text{ T}$ along the c-axis (0°). The orange curve shows the enhancement factor.



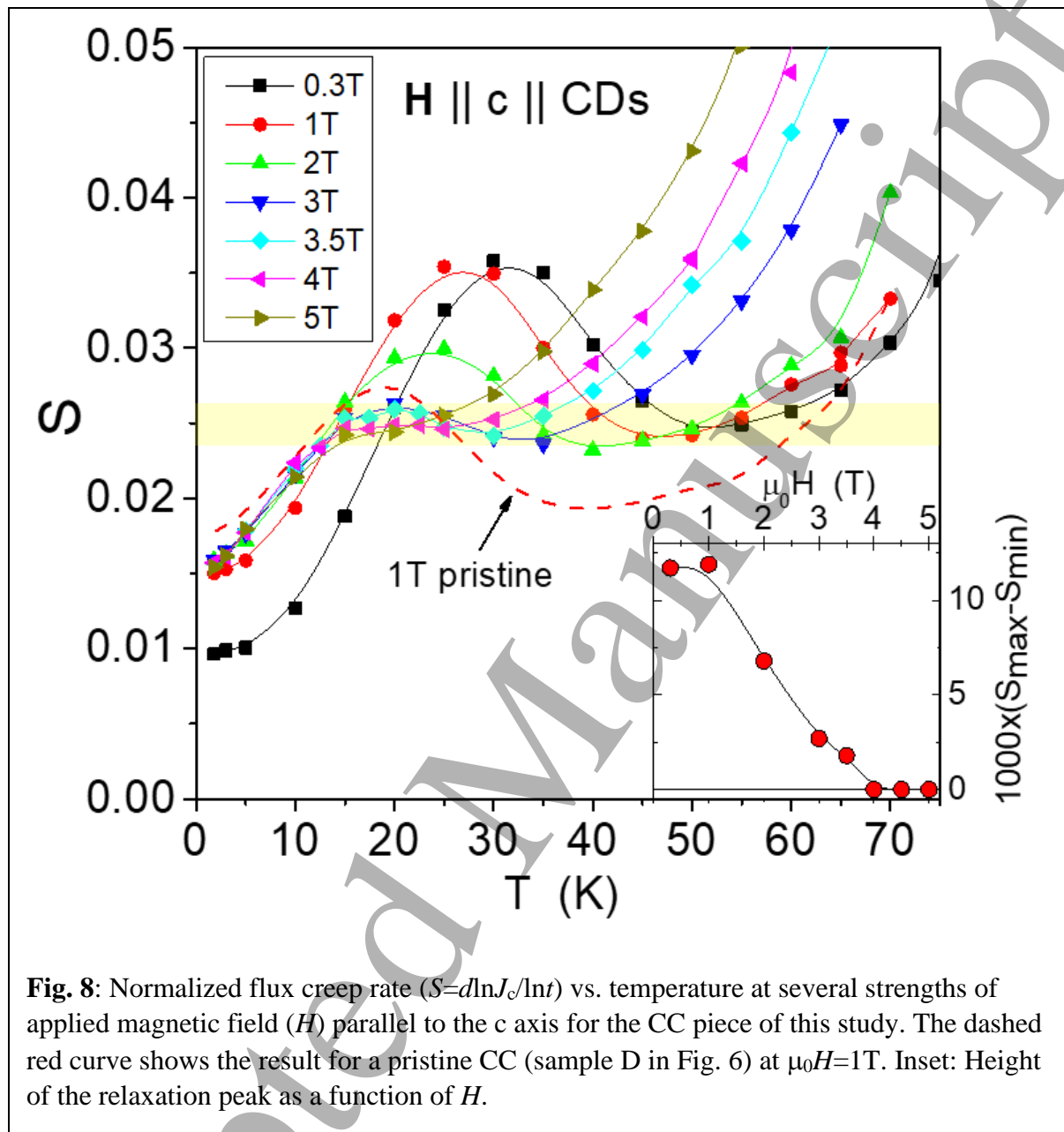


Fig. 8: Normalized flux creep rate ($S=d\ln J/\ln t$) vs. temperature at several strengths of applied magnetic field (H) parallel to the c axis for the CC piece of this study. The dashed red curve shows the result for a pristine CC (sample D in Fig. 6) at $\mu_0 H=1$ T. Inset: Height of the relaxation peak as a function of H .

- 1
2
3
4
5
6
7
8
9
10
11
12
13
14
15
16
17
18
19
20
21
22
23
24
25
26
27
28
29
30
31
32
33
34
35
36
37
38
39
40
41
42
43
44
45
46
47
48
49
50
51
52
53
54
55
56
57
58
59
60
-
- ¹ A.P. Malozemoff, *Annu. Rev. Mater. Res.* **42**, 373 (2012).
² Y. Shiohara *et al.*, *Jpn. J. Appl. Phys., Part 1* **51**, 010007 (2012).
³ X. Obradors and T. Puig, *Supercond. Sci. Technol.* **27**, 044003 (2014).
⁴ H. W. Weijers, W. D. Markiewicz, A. J. Voran, S. R. Gundlach, W. R. Sheppard, B. Jarvis, Z. L. Johnson, P. D. Noyes, J. Lu, H. Kandel, H. Bai, A. V. Gavrilin, Y. L. Viouchkov, D. C. Larbalestier, and D. V. Abraimov, *IEEE Trans. Appl. Supercond.* **24**, 1 (2014).
⁵ C. Senatore, M. Alessandrini, A. Lucarelli, R. Tediosi, D. Uglietti, and Y. Iwasa, *Supercond. Sci. Technol.* **27**, 103001 (2014).
⁶ D. Kramer, *Physics Today* **71**, 25 (2018).
⁷ S. R. Foltyn, L. Civale, J. L. MacManus-Driscoll, Q. X. Jia, B. Maiorov, H. Wang, and M. Maley, *Nat. Mat.* **6**, 631 (2007).
⁸ J. L. MacManus-Driscoll, S. R. Foltyn, Q. X. Jia, H. Wang, A. Serquis, L. Civale, B. Maiorov, M. E. Hawley, M. P. Maley, and D. E. Peterson, *Nat. Mat.* **3**, 439 (2004).
⁹ T. Haugan, P. N. Barnes, R. Wheeler, F. Meisenkothen, and M. Sumption, *Nature* **430**, 867 (2004).
¹⁰ Yamada, K. Takahashi, H. Kobayashi, M. Konishi, T. Watanabe, A. Ibi, T. Muroga, S. Miyata, T. Kato, T. Hirayama, Y. Shiohara, *Appl. Phys. Lett.* **87**, 132502 (2005).
¹¹ S. Kang, A. Goyal, J. Li, A. A. Gapud, P. M. Martin, L. Heatherly, J. R. Thompson, D. K. Christen, F. A. List, M. Paranthaman, and D. F. Lee, *Science* **311**, 1911 (2006).
¹² J. Gutierrez, A. Llodes, J. Gazquez, M. Gibert, N. Roma, S. Ricart, A. Pomar, F. Sandiumenge, N. Mestres, T. Puig, and X. Obradors, *Nat. Mat.* **6**, 367 (2007).
¹³ T. G. Holesinger, L. Civale, B. Maiorov, D. M. Feldmann, J. Y. Coulter, D. J. Miller, V. A. Maroni, Z. Chen, D. C. Larbalestier, R. Feenstra, X. Li *et al.*, *Adv. Mater.* **20**, 391 (2008).
¹⁴ P. Mele, K. Matsumoto, T. Horide, A. Ichinose, M. Mukaida, Y. Yoshida, S. Horii, and R. Kita, *Supercond. Sci. Technol.* **21**, 032002 (2008).
¹⁵ B. Maiorov, S. A. Baily, H. Zhóu, O. Ugurlu, J. A. Kennison, P. C. Dowden, T. G. Holesinger, S. R. Foltyn, and L. Civale, *Nat. Mat.* **8**, 398 (2009).
¹⁶ M. W. Rupich, X. Li, C. Thieme, S. Sathyamurthy, S. Fleshler, D. Tucker, E. Thompson, J. Schreiber, J. Lynch, D. Buczek, K. DeMoranville *et al.*, *Supercond. Sci. Technol.* **23**, 014015 (2010).
¹⁷ M. Miura *et al.*, *PRB* **83**, 184519 (2011); *Supercond. Sci. Technol.* **26**, 035008 (2013); *Sci. Rep.* **6**, 20436 (2016); *NPG Asia Materials* **9**, e447 (2017).
¹⁸ H. Tobita, K. Notoh, K. Higashikawa, M. Inoue, T. Kiss, T. Kato, T. Hirayama, M. Yoshizumi, T. Izumi, and Y. Shiohara, *Supercond. Sci. Technol.* **25**, 062002 (2012).
¹⁹ A. Xu *et al.*, *APL Materials* **2**, 046111 (2014); *ibid Sci. Rep.* **7**, 6853 (2017), 10.1038/s41598-017-06881-x.
²⁰ V. Selvamanickam, M. H. Gharahcheshmeh, A. Xu, Y. Zhang, and E. Galstyan, *Supercond. Sci. Technol.* **28**, 072002 (2015); V. Selvamanickam, M. H. Gharahcheshmeh, A. Xu, E. Galstyan, L. Delgado, and C. Cantoni, *Appl. Phys. Lett.* **106**, 032601 (2015); G. Majkic, R. Pratap, A. Xu, E. Galstyan, V. Selvamanickam, *Sci. Reports* **8**, 6982 (2018).
²¹ <http://fs.magnet.fsu.edu/~lee/plot/plot.htm>.
²² I. A. Sadovskyy, Y. Jia, M. Leroux, J. Kwon, H. Hu, L. Fang, C. Chaparro, S. Zhu, U. Welp, J. M. Zuo, Y. Zhang, R. Nakasaki, V. Selvamanickam, G. W. Crabtree, A. E. Koshelev, A. Glatz, W.-K. Kwok, *Advanced Materials* **28**, 4593 (2016).

- 1
2
3
4
5
6
7
8
9
10
11
12
13
14
15
16
17
18
19
20
21
22
23
24
25
26
27
28
29
30
31
32
33
34
35
36
37
38
39
40
41
42
43
44
45
46
47
48
49
50
51
52
53
54
55
56
57
58
59
60
-
- ²³ B. Maiorov, T. Katase, I.O. Usov, M. Weigand, L. Civale, H. Hiramatsu, and H. Hosono, *Phys. Rev. B* **86**, 094513 (2012).
- ²⁴ W.-K. Kwok, U. Welp, A. Glatz, A. E. Koshelev, K. J. Kihlstrom, *Rep. Prog. Phys.* **79**, 116501 (2016).
- ²⁵ Y. Zhu, Z. X. Cai, R. C. Budhani, M. Suenaga, D. O. Welch, *Phys. Rev. B* **48**, 6436-6450 (1993).
- ²⁶ M. A. Kirk, *Cryogenics* **33**, 235-242 (1993).
- ²⁷ M. Toulemonde, S. Bouffard, F. Studer, *Nuclear Instruments and Methods in Physics Research B* **91**, 108-123 (1994).
- ²⁸ Y. Yan, M. A. Kirk, *Phys. Rev. B* **57**, 6152-6164 (1998).
- ²⁹ M. A. Kirk, Y. Yan, *Micron* **30**, 507-526 (1999).
- ³⁰ M. Lang, R. Devanathan, M. Toulemonde, Ch. Trautmann, *Current Opinion in Solid State and Materials Science* **19**, 39-48 (2015).
- ³¹ I. A. Sadovskyy, A. E. Koshelev, A. Glatz, V. Ortalan, M. W. Rupich, M. Leroux, *Phys. Rev. Appl.* **5**, 014011 (2016).
- ³² G. Ghigo, F. Laviano, R. Gerbaldo and L. Gozzelino, *Supercond. Sci. Technol.* **25**, 115007 (2012).
- ³³ L. Civale, A. D. Marwick, M. W. McElfresh, T. K. Worthington, A. P. Malozemoff, F. H. Holtzberg, J. R. Thompson, M. A. Kirk, *Phys. Rev. Lett.* **65**, 1164 (1990); R. B. van Dover, E. M. Gyorgy, A. E. White, L. F. Schneemeyer, R. J. Felder, a J.V. Waszczak, *Appl Phys. Lett.* **56**, 2681 (1990)
- ³⁴ J. Giapmtzakis, W. C. Lee, J, P. Rice, D. M. Ginsberg, I. M. Robertson, R. Wheeler, M.A. Kirk, and M.O. Ruault, *Phys. Rev. B* **45**, 10677 (1992)
- ³⁵ A. Umezawa, G. W. Crabtree, J. Z. Liu, H. W. Weber, W. K. Kwok, L. H. Nunez, T. J. Moran, C.H. Sowers, and H. Claus, *Phys. Rev. B* **36**, 7151 (1987); F. M. Sauerzopf, H. P. Wiesinger, W. Kritscha, H. W. Weber, G. W. Crabtree, and J. Z. Liu, *Phys. Rev. B* **43**, 3091 (1991); H. W. Weber, in *Progress in High Temperature Superconductivity- Vol. 31* (World Scientific, Singapore, 1992)
- ³⁶ L. Civale, A. D. Marwick, T. K. Worthington, M. A. Kirk, J. R. Thompson, L. Krusin-Elbaum, Y. Sun, J. R. Clem, F. Holtzberg, *Phys. Rev. Lett.* **67**, 648 (1991).
- ³⁷ M. Konczykowski, F. Rullier-Albenque, E. R. Yacoby, A. Shaulov, Y. Yeshurun, and P. Lejay, *Phys. Rev. B* **44**, 7167 (1991).
- ³⁸ F. Laviano, R. Xie, E. Mezzetti and W.-K. Kwok, *Phys. Rev. B* **77**, 214501 (2008).
- ³⁹ Y. Jia, M. LeRoux, D. J. Miller, J. G. Wen, W. K. Kwok, U. Welp, M. W. Rupich, X. Li, S. Sathyamurthy, S. Fleshler, A. P. Malozemoff, A. Kayani, O. Ayala-Valenzuela, and L. Civale, *Appl. Phys. Lett.* **103**, 122601 (2013).
- ⁴⁰ M. Leroux, K. J. Kihlstrom, S. Holleis, M. W. Rupich, S. Sathyamurthy, S. Fleshler, H. P. Sheng, D. J. Miller, S. Eley, L. Civale, A. Kayani, P. M. Niraula, U. Welp, and W.-K. Kwok, *Appl. Phys. Lett.* **107**, 192601 (2015).
- ⁴¹ M. W. Rupich, S. Sathyamurthy, S. Fleshler, Q. Li, V. Solovyov, T. Ozaki, U. Welp, W.-K. Kwok, M. Leroux, A. E. Koshelev, D. J. Miller, K. Kihlstrom, L. Civale, S. Eley, and A. Kayani, *IEEE Trans. Appl. Supercond* **26**, 6601904 (2016).
- ⁴² S. Eley, M. Leroux, M.W. Rupich, D.J. Miller, H. Sheng, P.M. Niraula, A. Kayani, U. Welp, W-K. Kwok, and L. Civale, *Supercond. Sci. Technol.* **30**, 015010 (2017).

- 1
2
3
4
5
6
7
8
9
10
11
12
13
14
15
16
17
18
19
20
21
22
23
24
25
26
27
28
29
30
31
32
33
34
35
36
37
38
39
40
41
42
43
44
45
46
47
48
49
50
51
52
53
54
55
56
57
58
59
60
-
- ⁴³ K. J. Leonard, T. Aytug F. A. List, III, A. Perez-Bergquist, W. J. Weber, A. Gapud, Fusion Reactor Materials Program, June 30, DOE/ER-0313/54, Vol. 54, p. 125 (2013).
- ⁴⁴ K. J. Leonard, T. Aytug F. A. List, III, A. Perez-Bergquist, W. J. Weber, A. Gapud, Fusion Reactor Materials Program, December 31, DOE/ER-0313/55, Vol. 55, p. 54 (2013).
- ⁴⁵ K. J. Leonard, T. Aytug, A. Gapud, F. A. List III, N. T. Greenwood Y. W. Zhang, A. G. Perez-Bergquist, W. J. Weber, Fusion Science and Technology 66, 57 (2014).
- ⁴⁶ J. Hua, U. Welp, J. Schlueter, A. Kayani, Z. L. Xiao, G. W. Crabtree and W. K. Kwok, Phys. Rev. B **82**, 024505 (2010); K. J. Kihlstrom, L. Fang, Y. Jia, B. Shen, A. E. Koshelev, U. Welp, G. W. Crabtree, W.-K. Kwok, A. Kayani, S. F. Zhu, and H.-H. Wen, Appl. Phys. Lett. **103**, 202601 (2013).
- ⁴⁷ M. W. Rupich, D. T. Verebelyi, W. Zhang, T. Kodenkandath, and X. Li, MRS Bull. **29**, 572 (2004); X. Li, M. W. Rupich, C. L. H. Thieme, M. Teplitsky, S. Sathyamurthy, E. Thompson, D. Buczek, J. Schreiber, K. DeMoranville, J. Lynch, J. Inch, D. Tucker, R. Savoy, and S. Fleshler, IEEE Trans. Appl. Supercond. **19**, 3231 (2009); M. W. Rupich *et al.*, IEEE Trans. Appl. Supercond. **23**, 6601205 (2013).
- ⁴⁸ C. P. Bean, Rev. Mod. Phys. **36**, 31 (1964).
- ⁴⁹ A. E. Koshelev, I. A. Sadovskyy, C. L. Phillips, A. Glatz, Phys. Rev. B 93, 060508 (2016); R. Willa, A. E. Koshelev, I. A. Sadovskyy, A. Glatz, Supercond. Sci. Technol. 31, 014001 (2018).
- ⁵⁰ T. Hwa, P. Le Doussal, D. R. Nelson, and V. M. Vinokur, Phys. Rev. Lett. **71**, 3545 (1993).
- ⁵¹ L. Civale, L. Krusin-Elbaum, J.R. Thompson, R. Wheeler, A. D. Marwick, M. A. Kirk, Y. R. Sun, F. Holtzberg and C. Field, Phys. Rev. B **50**, 4102 (1994)
- ⁵² L. Civale, Supercond. Sci. Technol. **10**, A11 (1997).
- ⁵³ P.W. Anderson and Y.B. Kim, Rev. Mod. Phys. **36**, 39 (1964)
- ⁵⁴ G. Blatter, M.V. Feigel'man, V.B. Geshkenbein, A.I. Larkin and V.M. Vinokur, Rev. Mod. Phys. **66**, 1125 (1994)
- ⁵⁵ Y. Yeshurun, A.P. Malozemoff and A. Shaulov, Rev. Mod. Phys. **68**, 911 (1996)
- ⁵⁶ M.P.A. Fisher, Phys. Rev. Lett. **62**, 1415 (1989)
- ⁵⁷ M.V. Feigel'man, V.B. Geshkenbein, A.I. Larkin and V.M. Vinokur, Phys. Rev. Lett. **63**, 2303 (1989)
- ⁵⁸ N. Haberkorn, M. Miura, J. Baca, B. Maiorov, I. Usov, P. Dowden, S. R. Foltyn, T. G. Holesinger, J. O. Willis, K. R. Marken, T. Izumi, Y. Shiohara, and L. Civale, Phys. Rev. B **85**, 174504 (2012)
- ⁵⁹ D.R. Nelson and V.M. Vinokur, Phys. Rev. Lett. **68**, 2398 (1992)
- ⁶⁰ S. Eley, M. Miura, B. Maiorov and L. Civale, Nat. Mat. **16**, 409 (2017)
- ⁶¹ A.P. Malozemoff and M.P.A. Fisher, Phys. Rev. B **42**, 6784 (1990)
- ⁶² J.R. Thompson, L. Krusin-Elbaum, L. Civale, G. Blatter and C. Feild, Phys. Rev. Lett. **78**, 3181 (1997)
- ⁶³ D. Niebieskikwiat, L. Civale, C.A. Balseiro and G. Nieva, Phys. Rev. B **61**, 7135 (2000)
- ⁶⁴ M. Miura, B. Maiorov, S. Baily, N. Haberkorn, J. Willis, K. Marken, T. Izumi, Y. Shiohara and L. Civale, Phys. Rev. B **83**, 184519 (2011)
- ⁶⁵ L. Krusin-Elbaum, L. Civale, J.R. Thompson, C. Feild, Phys. Rev. B **53**, 11744 (1996)
- ⁶⁶ M. Leroux, V. Mishra, J. P. C. Ruff, H. Claus, M.P. Smylie, C. Opagiste, P. Rodière, A. Kayani, G. D. Gu, J. M. Tranquada, W.-K. Kwok, Z. Islam, and U. Welp, PNAS, 116 (22) 10691-10697 (2019)